JOURNAL OF MATERIALS SCIENCE 23 (1988) 1829–1834

Characteristics of diamond regrowth in a synthetic diamond compact

J. C. WALMSLEY, A. R. LANG
H.H. Wills Physics Laboratory, University of Bristol, Tyndall Avenue, Bristol BS8 1TL, UK

A transmission electron microscopic study of a commercial sintered diamond compact is reported that identifies and characterizes the diamond that has regrown between the grains of the original diamond powder during the high-pressure, high-temperature manufacturing process of the compact. The majority of the original grains are strongly deformed whereas the regrown diamond shows little or no plastic deformation. The dislocations in diamond regrown between the original grains occur in low-angle boundaries and other configurations typical of grown-in dislocations in crystals. The manufacturing process involves infiltrating the diamond aggregate by molten cobalt, and the regrown diamond is characterized by the presence of cobalt inclusions in sizes ranging from a few tenths of a micrometre down to a few nanometres, possessing the same orientation and lattice parameter as the diamond host. Graphite inclusions also occur in regrown diamond, few in comparison with cobalt inclusions and in random orientation. The graphite crystals exhibit axial ratios, (c/a), lowered by several per cent due to the containment pressure exerted by the diamond host.

1. Introduction

Synthetic polycrystalline diamond is an important industrial material, combining the wear resistance and hardness of natural diamond with toughness and mechanical isotropy. It can be produced in reasonably large pieces (of order 1 cm^3) and can be formed into specific shapes for different applications such as cutting tools and wire-drawing dies. The properties, principles of manufacture and applications of sintered diamond and cubic boron nitride compacts have been reviewed by Wentorf *et al.* [1]. They point out the practical difficulties in achieving compaction of a mass of small particles endowed with high yield and fracture stresses. These particles might sustain local pressures up to megabar order where they come into contact, whilst pressure over most of their surfaces corresponds to that in the interstitial voids, and is effectively zero. In the case of diamond powders, the existence of high temperature (say 1400° C) in the absence of the hydrostatic pressure needed ($\sim$ 54 kbar or 5.4 GPa) to keep the diamond stable leads to rapid graphitization and a consequent filling up of the low-pressure voids with the low-density graphite formed. The diamond compacts we have studied were consolidated adjacent to a source of cobalt [2]. Upon melting, this metal infiltrates the voids between the diamond grains, dissolving the graphite. When the intergranular volume is at both high pressure and high temperature, dissolved carbon precipitates out as diamond, leading to considerable intergrowth between the original diamond grains. Some cobalt (about 8 vol %) is retained in the material, most of it residing in a continuous network lying in channels between diamond grains.

The plastically deformed original grains of diamond compacts exhibit slip and microtwinning to a striking degree, as shown by transmission electron microscopy (TEM) studies [3–5], and a generally similar development of microtwinning has been observed by TEM in cubic boron nitride compacts [6]. This paper is concerned with the microstructural characteristics of the recrystallized diamond contained in diamond compacts.

2. Experimental procedure

Our observations have been made on Syndite* polycrystalline diamond. This is produced from synthetic diamond powder by consolidation at pressures of about 60 kbar (6 GPa) and temperatures above 1400° C in the presence of cobalt. Grades produced from starting material with average grain sizes of 2, 10 and 25 μm have been examined. Specimens in the shape of squat cylinders 3 mm in diameter were provided by the manufacturer. These were spark-cut into slices with a thickness of a few hundred micrometres, which was then reduced to about 50 μm by mechanical polishing on a cast-iron scaife loaded with diamond powder. Final reduction to electron transparency was achieved by argon ion-beam bombardment of both faces of the slice. A Philips Type 430 electron microscope, operating up to 300 kV, was used in the TEM studies.

3. Observations

3.1. Distribution of diamond and cobalt

Fig. 1 is a low-magnification, overall view of a fairly thick region in a sample prepared from 10 μm grade

*A registered trademark of De Beers Industrial Diamond Division.

0022–2461/88 $03.00 + .12

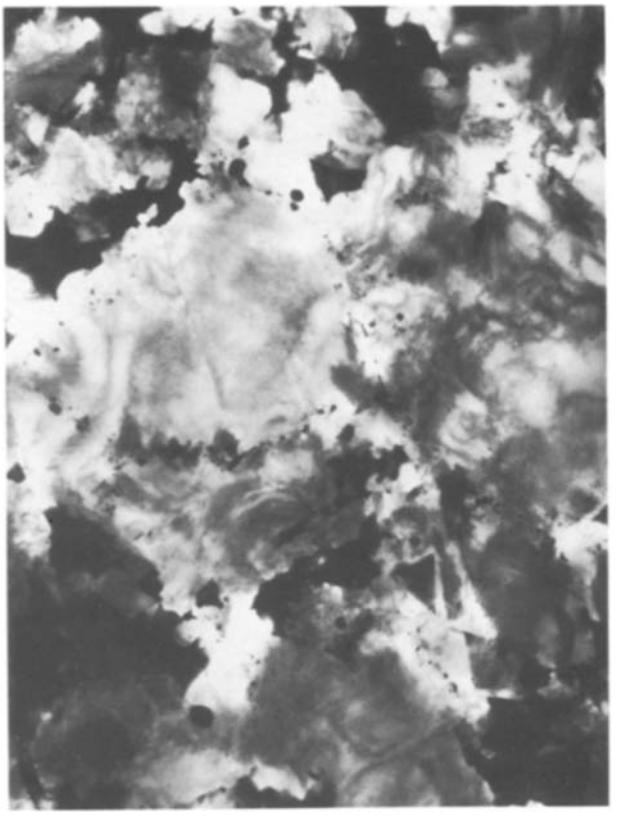

Figure 1 Low-magnification, bright-field micrograph showing distribution of diamond grains, their surrounding network of cobalt, and cobalt inclusions within diamond. Diamond grains in random orientation, thickness variable from $> 1\,\mu m$ down to zero. Field width $12.5\,\mu m$, electron accelerating voltage 300 kV.

material. It shows the distribution of diamond and cobalt, the metal generally appearing darker than the diamond due to its higher absorption of the electron beam. The larger masses of dark material correspond to the cobalt network threading the interstices between diamond grains, whilst discrete particles of metal can be discerned strung out along grain boundaries. In addition, small inclusions, sometimes recognisably faceted, appear within the diamond grains. The problem of uneven ion-beam thinning is evident. Exposed cobalt erodes comparatively rapidly. White areas on the print correspond to locations where the specimen has been thinned right through, and these are usually where metal was present. Any metal remaining around such holes is generally steeply wedged. In few localities in Fig. 1 can dislocations in the diamond grains be resolved individually, owing to the combined effects of high dislocation density and large diamond thickness. The variable darkness of images of the major diamond areas results mainly from local variations of diffraction conditions: much distortion of the larger grains is evident. Diamond grains sometimes show evidence of having cracked during the consolidation process. Some cracks contain cobalt whereas others appear to be clean. An apparently clean crack, its trace orientated 15° anticlockwise from the vertical, crosses the large grain section that forms the pale area centred a little above and to the left of the micrograph centre in Fig. 1. Generally the cobalt matrix is not found to be locally in parallel orientation with the diamond grains with which it has an interface. In fact, areas of cobalt surrounding several neighbouring grains, at least in the case of "002" and "010" grades (which have the smaller mean diamond particle diameters, 2 and $10\,\mu m$, respectively), will often go in and out of diffraction contrast simultaneously as the specimen is tilted. Closer examination confirms that a common orientation is present. In other words, the grain size of the metal network is actually larger than that of the diamond in the compact.

3.2. Identification of regrown diamond

Distinction between original and regrown diamond is not easy in low-magnification images of generally thick specimens like that in Fig. 1, but becomes much clearer in fields such as Fig. 2a. Here regrown diamond is seen bridging a gap $\sim 1.5\,\mu m$ wide between two dislocation-rich original grains that lie in the upper right and lower left parts of the field, respectively. Volumes of diamond characterized by a low dislocation density have grown on to the original grains and occupy the middle of the field, meeting in a high-angle grain boundary. The sample has been tilted so that both grains are exhibiting good diffraction contrast. The grain boundary is quite irregular, and there is no simple orientation relationship, approximate or exact, between the grains on either side of it. The boundary is simply the surface at which the regrowth fronts expanding from the original grains met during manufacture of the compact. This example can be taken as typical of diamond–diamond boundaries observed in

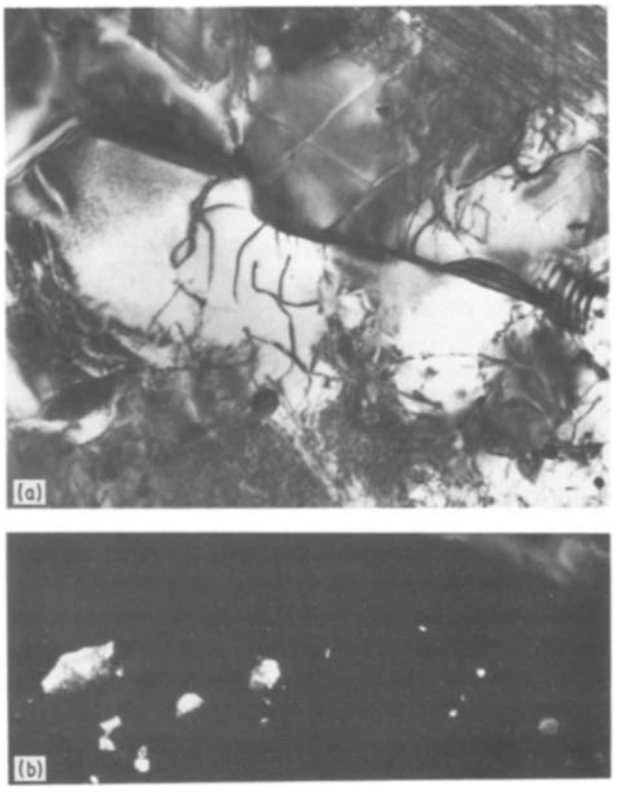

Figure 2 (a) A region containing typical low-dislocation-density regrown diamond, with a high-angle grain boundary crossing the field from above mid-height on left to below mid-height on right. Field width $2.6\,\mu m$, electron accelerating voltage 300 kV. (b) Dark-field image, cobalt 200 reflection, of lower half of field in (a) showing cobalt inclusions strongly diffracting.

specimens of the material studied. In both grains the transition from deformed original to regrown crystal is marked by a higher concentration of cobalt inclusions than is found further into the regrown region. This is a very general occurrence. The dark field image, Fig. 2b, formed by a 2 0 0-type "forbidden" reflection from the lower grain picks out the inclusions in that grain. They are strongly diffracting by virtue of their orientation relationship with the diamond enclosing them (as described in Section 3.3 below). These cobalt inclusions can also be recognised in Fig. 2a, but in that view their images are considerably masked by the dislocations close to them.

A small minority of original diamond grains in the compact have escaped heavy deformation and may possess quite a low density of glide dislocations. These grains are usually small compared with the average size, and may be of highly irregular shape. They are believed to be fracture fragments produced in the compaction process that have been sheltered from high shear stresses by the larger grains forming "arches" around them. In these relatively perfect grains one relies upon the presence of cobalt inclusions to indicate where regrown diamond commences. Dislocations may be generated at the inclusions and then be grown-in along trails roughly perpendicular to the advancing crystallization front.

3.3. Inclusions in regrown diamond

3.3.1. Cobalt

It is well known that synthetic diamonds contain metallic inclusions covering a wide range of sizes. They can be seen by optical microscopy and have been studied by X-ray diffraction [7, 8] and topography [9]. However, in the small synthetic diamonds used as starting material for the compact described here, metal inclusions are rare on the scale of probability of being captured in an electron microscope specimen. The very few examples found of metallic inclusions in the central parts of diamond grains were difficult to study because of the extreme deformation of the diamond matrix. Energy-dispersive X-ray spectroscopic analysis (EDS) showed the presence of iron and nickel in them. By contrast, the inclusions within the diamond matrix that are described here were found by EDS to contain cobalt plus a few per cent of tungsten, confirming their interpretation as being embedded in regrown rather than original material.

Fig. 3 shows two relatively large cobalt inclusions totally surrounded by regrown diamond. All the cobalt inclusions examined possessed the same lattice parameter and orientation relationship with the diamond as previously described [5], namely, the f c c β-cobalt has its lattice aligned parallel to that of the diamond host and contains enough interstitial carbon in solution for its lattice parameter to match that of diamond, to within the experimental accuracy of measurement in our electron diffraction patterns. This is identical behaviour to that found by Kohn and Eckart [8] in X-ray diffraction studies of cobalt contained in single-crystal diamonds grown in the cobalt–carbon system. In Fig. 3 the specimen has been tilted so that the electron beam direction is close to the [0 0 1] direction

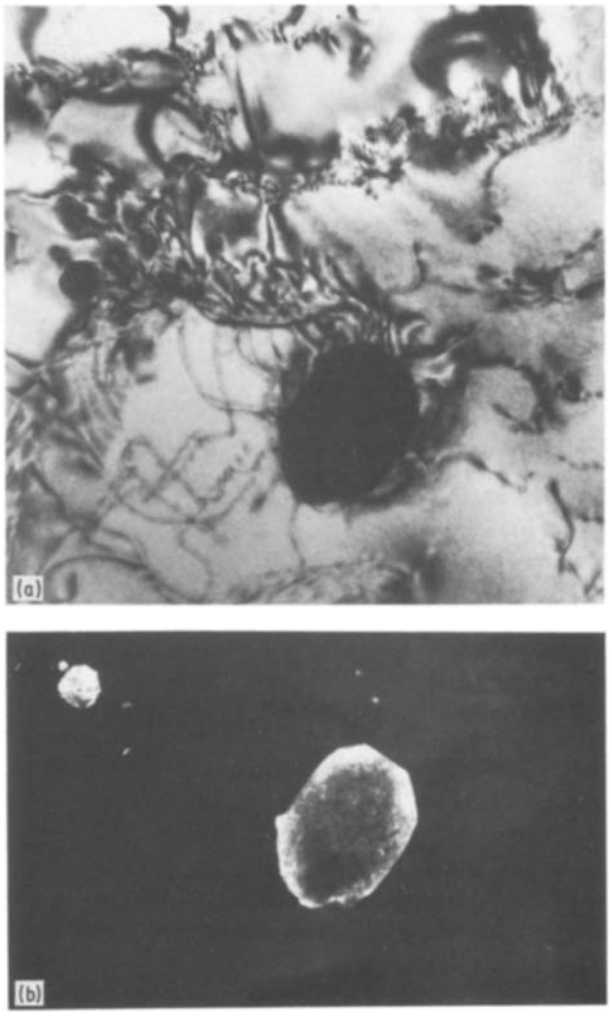

Figure 3 Regrown diamond containing cobalt inclusions. Both diamond and cobalt are close to [0 0 1] zone axis orientation. Field width 0.75 μm, electron accelerating voltage 300 kV. (a) 2 2 0 reflection, bright-field image. Cobalt inclusions appear dark (electron-opaque). Low-angle boundaries in the diamond cross the upper part of the field. (b) 2 0 0 reflection, dark-field image of lower two-thirds of field of (a). The larger cobalt inclusion, extreme dimension $\sim 0.2\,\mu$m in projection, shows high dislocation density.

in the diamond grain. There is then no zero-layer double-diffraction route to produce intensity in the kinematically-forbidden diamond 2 0 0-type reflections. However, 2 0 0 reflections are allowed in the cobalt f c c structure, so that dark-field images using this reflection show up oriented cobalt inclusions not easily seen in bright-field images. The electron diffraction pattern obtained with the orientation of Fig. 3 is shown in Fig. 4. In the bright-field image, Fig. 3a, the large inclusion appears dark due to its electron-opacity. Strong exposure in Fig. 3b shows that it has a high dislocation density. In Fig. 3a some strain contrast is present surrounding the large inclusion, but the great majority of cobalt inclusions produce no strain contrast in the diamond matrix. In the present case, the cavity in the diamond may be functioning as a local concentrator of long-range strain existing in this diamond grain.

Another feature commonly associated with regrown diamond is the presence of low-angle boundaries. Wavy low-angle boundaries appear in the upper part of Fig. 3a. No evidence has been found of polygonization

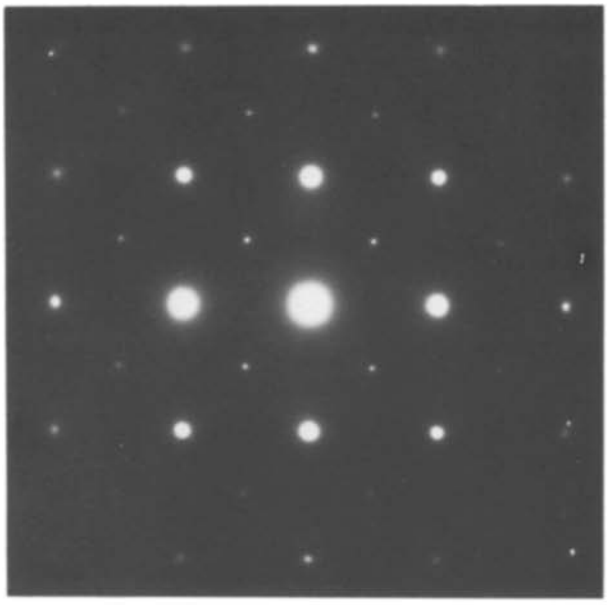

Figure 4 Diffraction pattern from an area containing both diamond matrix and the major inclusions of Fig. 3. The specimen is in [0 0 1] zone-axis orientation and the diffraction pattern is oriented with [1 1 0] pointing to the right. The faint inner four spots (forming a square with vertical sides) are the 2 0 0-type reflections from cobalt. Outside these are faint spots due to cobalt reflections of 4 2 0-type. The strong spots are overlapping diamond and cobalt reflections. Electron accelerating voltage 300 kV.

Figure 5 Group of graphite inclusions in regrown diamond. The largest (in the lower part of the field) is strongly diffracting; the overall width of its image is 0.2 μm. Another graphite inclusion, near the upper right corner of the field, is indicated by the arrow. A few smaller graphite inclusions can be detected, mainly by Fresnel fringe contrast. The largest graphite inclusion has a [1 0 $\bar{1}$ 0] direction approximately parallel to the electron beam and its *c*-axis is vertical on the print. Electron accelerating voltage 300 kV.

of dislocations in the strongly deformed cores of diamond grains, so that there is no reason to expect it to occur in the regrown outer layers. The low-angle boundaries are interpreted as grown-in features due to misorientations between adjacent areas of regrowth upon the same original grain.

The two major inclusions in Fig. 3b show facets corresponding to a cubo-octahedron in [0 0 1] projection. Whilst these facets represent the symmetry of the present solid cobalt it should be remembered that the cobalt was included while molten. Thus facets of the cavity occupied by cobalt reflect the symmetry of the diamond matrix: the cavities are "negative crystals" of diamond. Harris and Gurney [10] describe the morphology and orientation of mineral inclusions in natural diamond and discuss the not uncommon occurrence of diamond imposing its own morphology on various inclusion species. They remark that specific crystallographic orientations between inclusion and diamond are not a common phenomenon. Thus the exact parallel orientation between diamond and cobalt lattices found in synthetic material is an exceptional situation, by comparison with nature. The inclusions in Fig. 3, in particular the large one, have faces exhibiting some degree of curvature. After being enclosed by the growing diamond the cobalt should continue dissolving and reprecipitating carbon to produce the lowest-energy interface as long as it remains in the liquid state. However, it is not known in the present case whether the inclusion cavity was originally more or less spherical, with crystallographic facets developing subsequently, or whether the present form is the original form of the cavity.

3.3.2. Graphite

Compared with cobalt inclusions, graphite inclusions are difficult to detect. Firstly, they show low absorption contrast relative to the diamond matrix. Secondly, they are randomly oriented and so it is not possible to bring all or most of them in a given area into diffraction contrast simultaneously by tilting the matrix to a known orientation, as can be done with cobalt inclusions in the manner illustrated above. In number frequency, graphite inclusions are only a few per cent of cobalt inclusions. Fig. 5 shows a group of graphite inclusions. The specimen has been tilted so that the electron beam is approximately parallel to a [1 0 $\bar{1}$ 0]-type direction in the largest graphite crystal, seen in the lower part of the field, which is exhibiting strong diffraction contrast. This crystal has its *c*-axis normal to the lower horizontal edge of its image, which edge therefore represents an edge-on view of a basal plane facet. The general morphology of graphite inclusions is that of well-developed {0 0 0 1} facets and much less regular prism facets. Near the top right of the field is a smaller graphite inclusion. The arrow points at right angles to the centre of one of its basal-plane facets. This crystal is not in [1 0 $\bar{1}$ 0] axis orientation and is showing rather weak diffraction contrast except for a single bend contour. Its outline, like that of other, non-diffracting, graphite inclusions, can be picked out by Fresnel fringe contrast resulting from the difference in electron density between graphite and diamond combined with a slight image defocus. This smaller inclusion has a more regular morphology than the larger one. Both show some rounding of their facets. The diffraction contrast image of the larger inclusion indicates a columnar structure parallel to the *c*-axis.

Figs 6 and 7 show selected-area diffraction patterns from the largest inclusion in Fig. 5. In Fig. 6 the beam

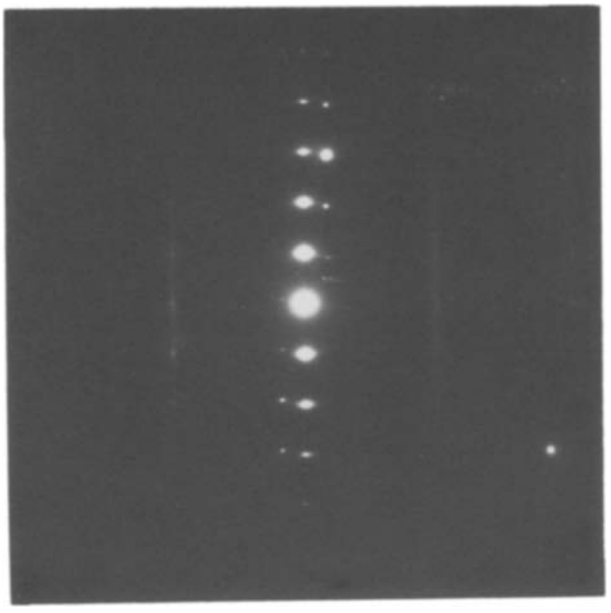

Figure 6 Diffraction pattern from the largest graphite inclusion in Fig. 5. The pattern is correctly oriented with respect to Fig. 5: the mean graphite [0 0 0 1] direction is vertical.

has included some material significantly misoriented with respect to the bulk of the crystal, as the row of $0\,0\,0\,l$ spots rotated clockwise with respect to the main diffraction pattern shows. The $1\,1\,\bar{2}\,l$ rows appear weak and streaked. Discrete reflections are only clear in the right-hand member of the pair. Some of this pattern imperfection is attributable to lack of alignment of the electron beam with the zone axis. A rotation of the specimen by 30° about the inclusion c-axis produced the much better $[1\,1\,\bar{2}\,0]$-type zone axis pattern shown in Fig. 7. Selected-area $[1\,1\,\bar{2}\,0]$ zone-axis patterns of some other inclusions were of similarly good quality. Axial ratios, (c/a), derived therefrom are shown in Table I, where their fraction of the zero-pressure value, (c_0/a_0), is related to pressure

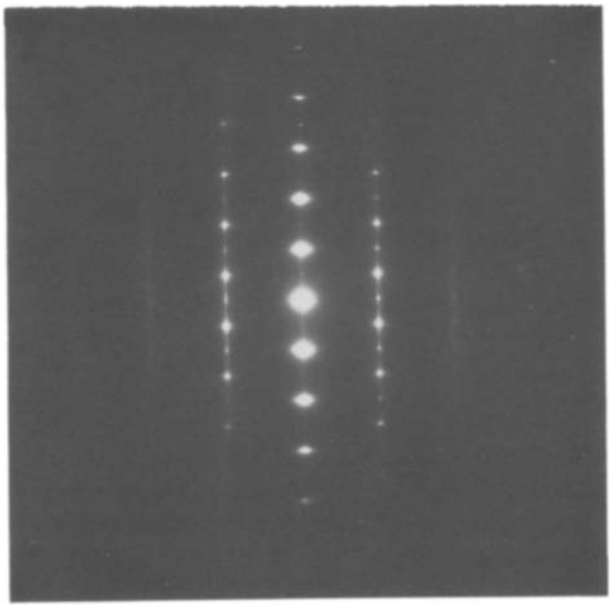

Figure 7 Diffraction pattern obtained from the same graphite inclusion by rotating the specimen 30° about the graphite [0 0 0 1] direction to obtain a $[1\,1\,\bar{2}\,0]$-type zone axis pattern. Weak, kinematically forbidden reflections appear along the $0\,0\,0\,l$ and $\pm 1\,0\,\bar{1}\,l$ rows due to double diffraction.

TABLE I Pressure on graphite inclusions: comparison of observed axial ratio (c/a) with zero-pressure value (c_0/a_0)

Inclusion	Observed (c/a)	$(c/a)/(c_0/a_0)$	Pressure (kbar)*
A	2.61	0.96	24
B	2.56	0.94	42
C	2.59 to 2.61	0.95 to 0.96	25 to 32
D	2.61 to 2.62	0.96	22 to 24
E	2.65	0.97	12

*10 kbar = 1 GPa.

using the data of Lynch and Drickamer [11]. (Those workers used $c_0 = 0.67078$ nm and $a_0 = 0.24612$ nm as graphite lattice parameters under normal laboratory temperature and pressure conditions, giving $(c_0/a_0) = 2.725$. Inclusion A in Table I is the largest inclusion in Fig. 5. In the diffraction patterns, measurements of the distance between the $1\,0\,\bar{1}\,l$ and $\bar{1}\,0\,1\,l$ rows could be made to a few parts in 10^3, but as regards measurements along the $0\,0\,0\,l$ row the patterns indicated that a range of c-values was present in the sample volume, sufficiently large to warrant stating it explicitly in Table I in two cases. (The $(c/a)/(c_0/a_0)$ ratios are rounded to two significant figures in the table.) The initial rate of reduction of (c/a) with increasing pressure is about 1% per 5 kbar (0.5 GPa) [11]. It is to be expected that the present inferred containing pressures of the graphite inclusions show a wide spread, since a thin-foil specimen can provide only imperfect containment. If one wished to attempt to discover from the figures in Table I the pressure on the graphite at the time of its inclusion one would have to allow for the difference between the high, anisotropic thermal expansion of graphite and the small, isotropic thermal expansion of diamond. Such allowance, for a drop from 1400° C to room temperature, would add about 20 kbar (2 GPa) to the pressures in the table, which at least produces no unlikely maximum value.

4. Conclusions

By the time the stage in the manufacturing process is reached at which diamond regrowth is proceeding, most of the deformation of the original diamond grains has already taken place and the shape of the compact is stable. So that when the texture of regrown diamond is examined electron-microscopically, it is found to have the characteristics of undeformed, or very little deformed crystal. The dislocation density is low and the majority of dislocations are grown-in, some being evidently associated with the inclusions of cobalt trapped by the advancing diamond growth front or at the interface between original and regrown diamond. The presence of such inclusions, having a wide range of sizes and always in parallel orientation with the diamond matrix, is an important identifying feature of regrown diamond. Less common in regrown diamond are graphite inclusions, randomly oriented. They are interpreted as relics of the graphitization stage, having escaped solution by the infiltrating molten cobalt. Qualitatively, little difference is found in the characteristics of diamond regrowth in compacts of different grades of grain size.

Almost complete exclusion of cobalt from large

areas where two grains have grown together is observed. No thin, residual layer of cobalt was detected at grain boundaries by the techniques employed, namely bright- and dark-field, and absorption-contrast imaging. The observation of widespread diamond-to-diamond bonding explains why the mechanical properties of the compact are essentially those of the original particles, and that leaching out the cobalt by acid causes only slight weakening.

Acknowledgements

We thank SERC for support, and Dr R. Caveney, De Beers Industrial Diamond Division (Pty) Ltd, for providing specimens.

References

1. R. H. WENTORF, R. C. DEVRIES and F. P. BUNDY, *Science* **208** (1980) 873.
2. P. N. TOMLINSON and R. J. WEDLAKE, in Proceedings of International Conference on Recent Developments in Specialty Steels and Hard Materials, edited by N. R. Comins and J. B. Clark (Pergamon, Oxford, 1983) p. 173.
3. J. C. WALMSLEY and A. R. LANG, *J. Mater. Sci. Lett.* **2** (1983) 785.
4. S. YAZU, T. NISHIKAWA, T. NAKAI and Y. DOI, in Proceedings of International Conference on Recent Developments in Specialty Steels and Hard Materials, edited by N. R. Comins and J. B. Clark (Pergamon, Oxford, 1983) p. 449.
5. J. C. WALMSLEY and A. R. LANG, in "Ultrahard Materials Application Technology", Vol. 3, edited by Paul Daniel (De Beers Industrial Diamond Division, Ascot, 1985) p. 11.
6. *Idem, J. Mater. Sci.* **22** (1987) 4093.
7. K. LONSDALE, H. J. MILLEDGE and E. NAVE, *Mineral. Mag.* **32** (1959) 185.
8. J. A. KOHN and D. W. ECKART, *Amer. Mineralogist* **47** (1962) 1422.
9. Y. KAMIYA and A. R. LANG, *J. Appl. Phys.* **36** (1965) 579.
10. J. W. HARRIS and J. J. GURNEY, in "The Properties of Diamond", edited by J. E. Field (Academic, London, 1979) Ch. 18, p. 555.
11. R. W. LYNCH and H. G. DRICKAMER, *J. Chem. Phys.* **44** (1966) 181.

Received 3 April
and accepted 16 June 1987